Polymer 51 (2010) 5221–5228

Contents lists available at ScienceDirect

Polymer

journal homepage: www.elsevier.com/locate/polymer

Ion-assisted collection of Nylon-4,6 electrospun nanofibers

Jan C. Uecker [a], Gary C. Tepper [a], Joan Rosell-Llompart [b,c,*]

[a] Department of Mechanical Engineering, Virginia Commonwealth University, 601 W Main Street, Richmond VA 23284, USA
[b] Department of Chemical Engineering, Universitat Rovira i Virgili, Avinguda dels Països Catalans 26, 43007 Tarragona, Spain
[c] ICREA (Catalan Institution for Research and Advanced Studies), Barcelona, Spain

ARTICLE INFO

Article history:
Received 27 November 2009
Received in revised form
20 August 2010
Accepted 30 August 2010
Available online 6 September 2010

Keywords:
Electrospinning
Nanofibers
Nylon-4,6

ABSTRACT

In electrospinning, electrostatic interaction between charged fibers and the collection substrate can result in poor and non-uniform coverage, particularly when electrically insulating substrates are used, because they are prone to surface charge accumulation. Charged electrospun Nylon-4,6 nanofiber coatings were deposited onto substrates of varying size, conductivity and morphology. The density and uniformity of the nanofiber coatings were significantly enhanced, both on insulating and on conducting substrates, by a new method based on rapid sequential deposition of charged nanofibers and oppositely charged ions onto substrates that were mounted onto a rotating collecting electrode (mandrel) located between an electrospinning source and a focused ion source. Sequential fiber/ion deposition presumably led to surface charge neutralization or reversed charging, and minimization of electrostatic fiber/substrate interactions. An electrostatics model was developed to interpret the experimental results. It was also theoretically argued that any degree of ion charging will induce continuous fiber accumulation.

1. Introduction

This work is concerned with the coating of surfaces with charged polymer nanofibers generated by electrospinning, and specifically, with overcoming electrostatic effects that result in non-uniformity of the fiber distribution. Electrospun fibers have been proposed for applications in diverse fields, such as nanofiltration [1,2], regenerative medicine [3–5], drug delivery [6–8], sensors [9], protective clothing [10,11], enzyme catalysis [12], nanofluidic devices [13], among others [14–18]. In the typical electrospinning process, the polymer solution is pumped through the end of a bare electrified capillary tube ('spinneret' or 'needle'), where it is then pulled into a thin liquid filament by the action of electrostatic stresses. As the charged filament flies away from the needle, it undergoes whipping motions caused by a bending instability [19–21].

Although the whipping causes fibers to deposit in random orientations over an electrically grounded collector plate, electrostatic phenomena localized over the substrate often lead to non-uniform distribution of the collected fibers. Non-uniform patterns of fibers have been described in the literature for conductive meshes [11,22–24], insulating meshes [24], and substrates having variable conductivity across the surface, such as for a dispersed conductive phase in an insulating matrix [11,25]. In any of these situations, fibers are generally preferentially attracted to higher conductivity regions, leading, for instance, to star patterns centered on conductive particles dispersed in a dielectric matrix [25]. Further examples of non-uniform patterns on both insulating and conducting mesh-like substrates are provided in this work.

Electrostatic charging of an insulating substrate (or a substrate having both conductive and insulating regions) is another often undesired effect, which results in fiber repulsion. In the course of this work, we have encountered electrostatic charging of insulating substrates $\sim$1 cm^2 in coverage area, mounted over a grounded electrode. Once insulating substrates become saturated with electrostatic charge, they stop admitting fibers, or, as permitted by charge loss, the rate of fiber collection rate drops significantly.

Both the localized fiber patterns mentioned earlier and the electrostatic charging resulting in fiber repulsion influence the motions and paths of airborne fibers near the substrate, in response to the spatial variations of the electrostatic field near the collector. In applications seeking highly uniform coatings, such as filtration, all these phenomena are undesirable.

The use of corona ions to neutralize substrate charging in electrospinning was previously suggested [22]. Also, Morozov and Vsevolodov used an electrospray to neutralize fibers during electrospinning formation of free and supported nanomats [24]. Corona ions have actually been used for discharging non-conducting

* Corresponding author. Department of Chemical Engineering, Universitat Rovira i Virgili, Avinguda dels Països Catalans 26, 43007 Tarragona, Spain. Tel.: +34 977 558 660; fax: +34 977 559 621.
E-mail address: joan.rosell@urv.cat (J. Rosell-Llompart).

0032-3861/$ – see front matter © 2010 Elsevier Ltd. All rights reserved.
doi:10.1016/j.polymer.2010.08.057

substrates while being coated by electrospray droplets from dilute polymer solutions (rather than electrospun fibers) [26,27]. In those electrospray studies, the polymer concentration in the starting solution was low enough to result in break up of the liquid into droplets soon after exiting the needle; thus precluding the electrospinning phenomenon, which occurs at much higher polymer concentrations (typically few percent by weight and higher).

In this work, we present a new method in which corona ions are deposited onto oppositely charged fibers supported on substrates of varying conductivity and morphology. The collection of corona ions by the substrate and the fibers results in highly uniform and planar deposition of electrospun fibers. The substrates are mounted onto an electrically grounded electrode which is rotated about an axis that is perpendicular to the electrospinning needle. During spinning, the filaments (fibers) are aimed at one side of the rotating collector, while ions of opposite polarity produced by a corona discharge are aimed at the other side of the collector. Because fiber whipping is not suppressed, randomly oriented fibers are still obtained, despite the rotation of the collector.

In addition, theoretical electrostatics arguments are used both to analyze the conditions leading to complete fibers rejection (in the absence of corona ions), and to analyze the situation created by the collection of corona ions. The question of whether residual charge on the fiber mat itself should lead to fiber rejection in standard electrospinning practice is also discussed.

2. Materials and methods

Nylon-4,6 was selected as a prototypical polymer because it has good mechanical properties and is compatible with the electrospinning process [28,29]. Our electrospinning solution was Nylon-4,6 ($T_m = 295$ °C, $\rho = 1.18$ g/ml, Sigma-Aldrich 442992) at various concentrations (19, 18, and 16 wt.%) in formic acid (98%, Fluka 06440), to which 0.4 wt.% of pyridine (99%, Sigma-Aldrich 360570) was added. Although this solution darkens over time, we did not observe any influence of aging on the electrospinning behavior after storage for one week at room temperature. Vials with solutions were stored in the refrigerator, and were discarded after one week.

Electrospun fibers were deposited onto various kinds of substrate materials cut in the form of sheets or discs, which were attached to an aluminum mandrel ("collection cylinder") of hexagonal cross section (Fig. 1 a). The collection cylinder was rotated at 1200 rpm (+/−5%). The electrospinning needle (23G [0.6 mm OD] stainless steel) and corona ion source were positioned on opposite sides of the collection cylinder as shown in Fig. 1a. A Harvard Apparatus PHD2000 infusion syringe pump was used to set the liquid flow rate at 0.4 μL/min, which slightly exceeded the flow rate of the electrospinning jet (estimated to be near 0.3 μL/min). Consequently, the droplet from which the Taylor cone emerged accumulated solution over time and was periodically wiped off. Because it is difficult to exactly match the syringe pump flow rate to the flow rate of the jet, we found it convenient to exceed the required flow rate in order to avoid depletion of the droplet and unanticipated interruption of the jet. The distance between the needle tip and the collection cylinder was fixed at 10 cm during all of the experiments reported here. In all of the tests, the whipping instability of the jet was observed to develop about 1–2 cm downstream from the needle tip [21].

The corona assembly (Fig. 1a and b) was comprised of a Teflon rod (19 mm dia.), a corona needle (beveled 21G SS capillary cut from a Becton Dickinson PrecisionGlide needle), and a corona shield (made of electroformed nickel mesh, 0.18 mm dia. wire welded in a square pattern with 4.5 × 4.5 mm^2 openings, and wrapped around the Teflon rod). The needle and the mesh

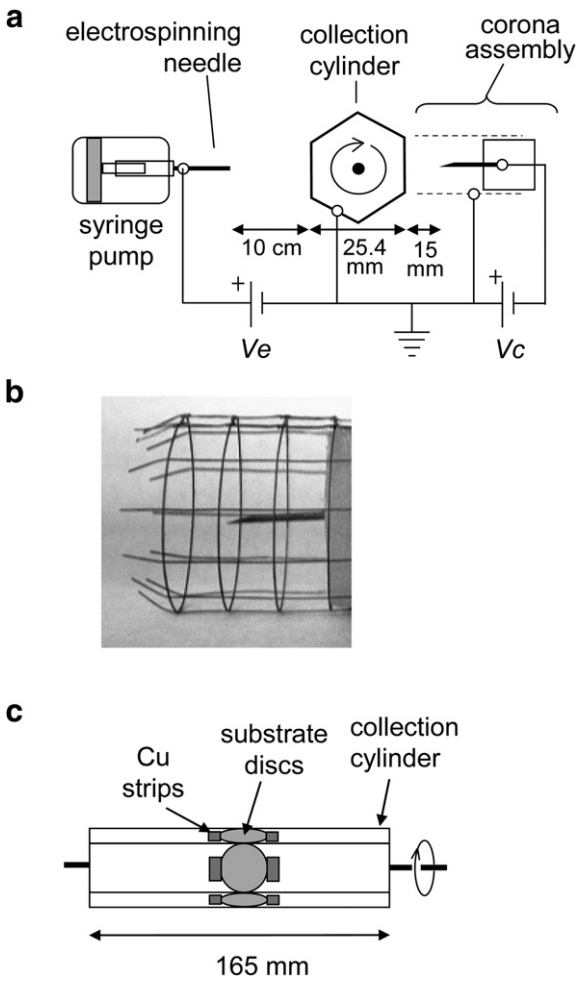

Fig. 1. (a) Schematic of electrospinning setup, (b) corona needle assembly, (c) mode of attachment of substrate discs.

protruded 9 and 18 mm axially from the Teflon rod, respectively. The assembly was positioned such that the distance between the needle tip and the flat side of the cylinder was 15 mm (see Fig. 1a). The corona shield was used to prevent ion leakage around the collection cylinder and in-flight neutralization of the oppositely charged electrospun fibers. Both the collection cylinder and the corona shield were electrically grounded.

A positive high voltage V_e, usually +7.5 kV, was supplied to the electrospinning needle from a Matsusada Precision Inc. model AMT-10B10-LCS power supply; whereas a negative high voltage V_c, usually −5 kV, was supplied to the corona needle from a Spellman model CZE1000R power supply, which provided an output voltage proportional to the supplied current ("corona current"). The jet envelope near the electrospinning needle (which is associated with the early stages of whipping [21]) was not visibly affected by corona conditions during the experiments.

The substrate materials tested are described in Table 1, which include woven meshes of polyester, fiberglass, nylon, and stainless steel, non-woven polyester, and solid glass. These materials were shaped as either (a) discs 12.7 mm (½") in diameter, or (b) strips of sheeting 8 cm wide. The discs were mounted onto different faces of the collection cylinder either as a set of 6 discs or of 2 discs (on opposite cylinder faces). The discs were attached to the cylinder using two short adhesive strips of copper tape on either side along the cylinder axis, as shown in Fig. 1c. The 8 cm wide strip was

Table 1
Characteristics[a] of substrate materials used.

Name	Material[b]	Cloth type	D_t (μm)[c]	Thread cross section	%OA[d]	S, (μm)[e]	W_o, (μm)
P-20[f]	P	Non-woven	20	Trilobal	N/A[g]	240	N/A
N-50	N	Square weave	50	Circular	36	82[h]	75
N-75	N	Square weave	75	Circular	33	125	100
N-120	N	Square weave	120	Circular	53	200	325
N-165	N	Square weave	165	Circular	37	245	260
N-305	N	Square weave	305	Circular	37	480	480
N-495	N	Square weave	495	Circular	44	845	985
P-225	P	Square weave	225	Circular	49	350	535
P-415	P	Square weave	415	Circular	45	720	835
F-340	F	Square-weave	340	Circular	59	365	1130
Glass disc	G	N/A	N/A	N/A	0	240	N/A
S-370	SS	Square weave	370	Circular	49	735	860

[a] D_f = Thread diameter; *%OA* = Percent open area; S = Substrate thickness; W_o = Opening width.
[b] P = Polyester; N = Nylon; F = Fiberglass; G = Glass; SS = Stainless steel.
[c] For polyester non-woven, the diameter is based on the denier per filament provided by the manufacturer (DPF = 4.0). For the rest, thread diameter is based on measurements taken on SEM micrographs.
[d] For square weave, *%OA*'s are from measurements taken on SEM micrographs of the substrates.
[e] Manufacturer's spec for "polyester non-woven"; other thicknesses are determined using a caliper, under as little load as possible.
[f] Reemay Fiberweb™ 2014.
[g] Basis weight for this material is 34 g/m^2.
[h] Extrapolated based on the other materials, as $1.62\times D_f$.

wrapped around the collection cylinder in a single layer and attached at the ends using double-sided scotch tape. The variation in ambient temperature across all runs was 22.5–25 °C, and of relative humidity 34%–46%. Fiber adhesion was only good to nylon substrates, suggesting that enough solvent remains on the collected fibers to "weld" them to the nylon substrate.

The collected fibers were not post processed (heated or dried) and were imaged using a Zeiss EVO 50 scanning electron microscope SEM (30 kV). Unless noted otherwise, the images are from the central part of the deposition region. IrfanView version 4.10 was used to adjust image settings (brightness and contrast in all cases, and gamma in a few cases, as noted).

3. Results and discussion

3.1. Charge saturation of electrically insulating substrates

Electrospinning directly onto discs of various insulating materials caused poor and irregular fiber coverage. Fig. 2a and b show examples onto non-woven polyester P-20 substrate discs 12.7 mm in diameter (Table 1). After spinning for 10 min, fiber collection over the discs was unnoticeable by eye, whereas a clearly visible film had formed just outside of the discs on the neighboring conducting surfaces of the cylinder, spreading about 2 cm to either side of the band of discs (Fig. 1c). Fig. 2a shows the region near the edge of a P-20 disc (disc at the right side of the image). In this experiment, prior to spinning, the grounded cylinder had been covered with aluminum foil to allow transferring surrounding fibers to the SEM for observation. It can be seen that fiber coverage over the aluminum sheet surrounding the non-woven substrate disc is much denser than directly over the disc, where very few fibers can be observed. In these and other experiments with discs, a narrow gap devoid of fibers surrounding the discs was visible by naked eye, and is also visible in Fig. 2a. Fig. 2b is a higher magnification image of the center region of a polyester disc, and shows a sparse layer of nanofibers about 200 nm in diameter over the much thicker threads of the substrate. The fiber concentration in this central disc region was found to be somewhat higher than closer to the edge of the disc, but much lower than outside of the disc. Discs occupied 3% of the collection area (including the discs), yet only accumulated 0.5% of the fiber mass or less. A similarly low level of fibers could be collected onto N-165 mesh discs and onto glass discs (Table 1).

These observations are indicative of electrostatic charging by initial fibers and subsequent repulsion of additional fibers, which are deflected away from the substrate towards the surrounding areas. The electrostatics model presented next lends some support to this view.

3.2. Charge saturation conditions for complete fiber rejection

Electrostatic charge carried by electrospun fibers to a perfectly insulating substrate should accumulate over time until a saturation level is reached. For an imperfectly insulating substrate, this saturation level of residual charge is not actually reached because of charge losses (by conduction, for instance). The saturation level is, therefore, the maximum charge attainable, and is reached when the electrostatic field due to the charges on the substrate $\vec{E}_s$ cancels out the external field $\vec{E}_o$ that drives the electrospinning and fiber transport processes. Under this scenario, the accumulated charge saturates and airborne fibers are repelled. Because the dependence of $\vec{E}_s$ on the surface charge density σ (coulombs/m^2) is known, and $\vec{E}_o$ is determined mostly by the electrodes shapes and their potentials, an estimate of the maximum attainable surface charge density $\sigma_{\max}$ can be obtained by equating the two field strengths: $E_s = E_o$.

The sources of $\vec{E}_s$ include not only (i) the charges bound to the collected fibers ("free charges"), but also (ii) "polarization charges" on the dielectric layer, and (iii) the charges induced on the metal surface (assumed to be planar and have infinite extent) by the fiber and polarization charges (modeled as "image charges" located inside the metal). We model this distribution as two thin discs of uniform positive and negative charge (a double layer) that sandwich a linear polarizable material with a uniform dielectric constant equal to that of the substrate, ε, and is twice as thick as the substrate. The magnitude of $\vec{E}_s$ along the axis ($r = 0$) can be obtained by integration of Coulomb's law using the dipolar approximation:

$$E_s(z,t) \approx \frac{\sigma(t)}{\varepsilon\varepsilon_o}\frac{S}{R}\frac{1}{m\left[1+\left(\frac{z}{R}\right)^2\right]^n} \quad (z >> S;\ r = 0) \tag{1}$$

Here, z and r are cylindrical coordinates, with z running perpendicular to the substrate circular disc with origin at the metal surface of the grounded electrode, r being the radial coordinate from the disc axis, R is the substrate disc radius, S its thickness, t is time, $\sigma(t)$ is the surface density of free charge (C/m^2), which grows with time t due to fiber accumulation and is assumed to be uniform over the substrate (independent of r), ε_o is the vacuum permittivity (8.854×10^{-12} F/m), and m and n are constants, which depend on geometry, with $m = 1$, $n = 3/2$ for a circular disc. Expression (1) is valid provided z remains much larger than S, as required by the dipolar approximation.

For a needle tip (assumed to be centered on the disc) positioned at a distance L from the substrate that is much greater than R (say $L \geq 10\times R$), E_o is approximately uniform over the substrate, and is of order V_e/L, where V_e is the needle voltage. Equation (1) can be solved for $\sigma_{\max}$, after taking it for $z = 0$, and equating E_s with $E_o \approx V_e/L$:

$$\sigma_{\max} \approx \varepsilon\varepsilon_o\frac{V_e}{L}\frac{R}{S} \tag{2}$$

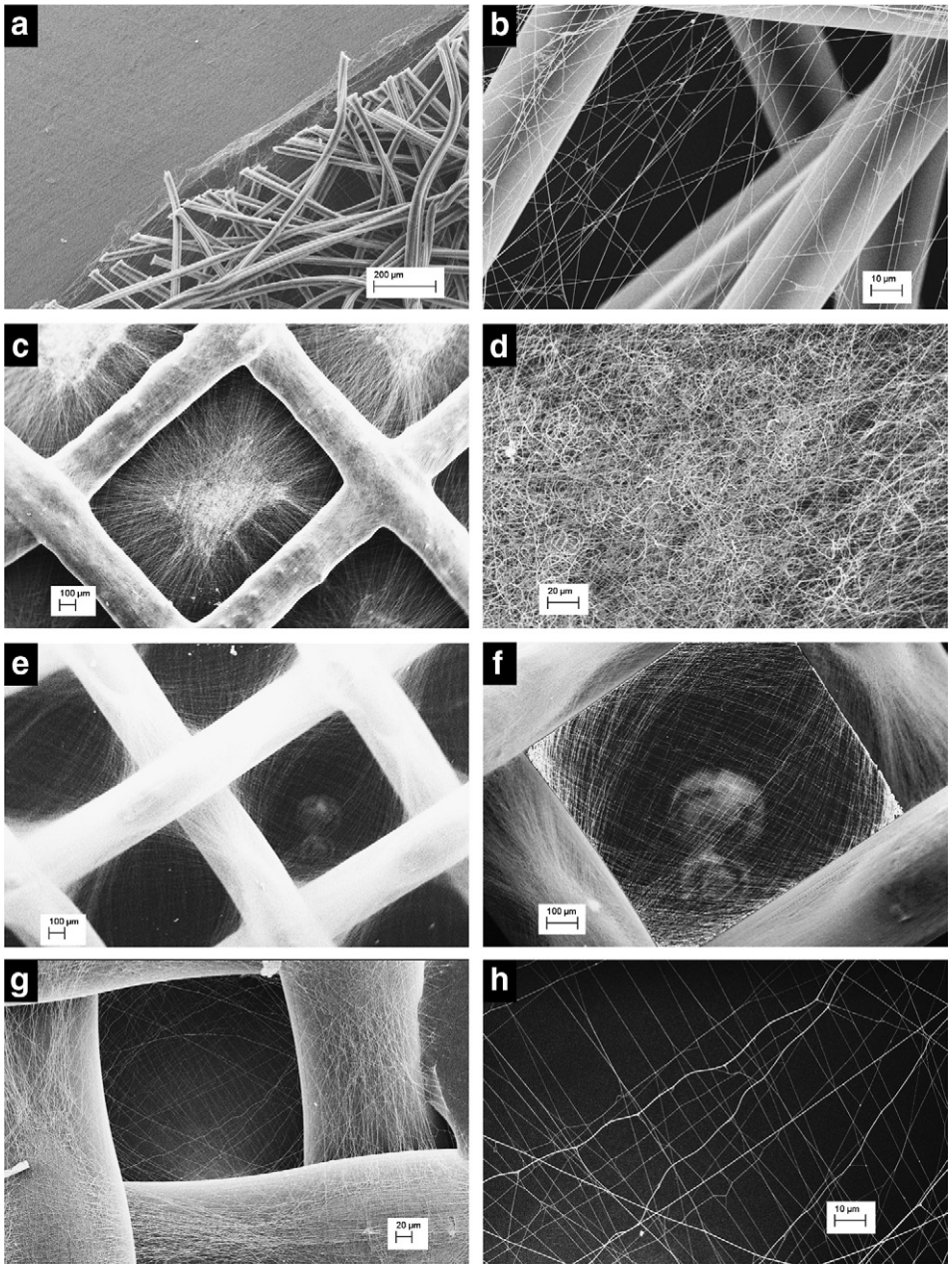

Fig. 2. SEM images of electrospun nylon fibers collected in absence of ion assistance onto different substrates: (a) two P-20 discs; (b) six P-20 discs; (c, d) two F-340 discs; (e, f) two S-370 discs; (g) N-165 8-cm wide strip (center of deposition region); (h) detail of (g). Nylon solution concentrations: 19% wt (a), 18% wt (c, d, e, f), 16% wt (b, g, h). Collection times: 10 min (*a*)–(f), 5 min (*g*, h). $V_e = +7.5$ kV; $V_c = 0$. (In 2f different image settings were used for the open square as for the mesh wires; for the latter, gamma = 0.14. For image 2g, gamma = 0.70).

Note that a different choice of z would have changed this expression only slightly, since E_s in eq. (1) varies slowly with z for $z < R$.

The σ_{max} computed using (2) at the experimental conditions corresponding to Fig. 2b ($S = 0.24$ mm, $R = 12.7$ mm, $V_e = 7500$ V, $L = 0.1$ m) lies between 1.8×10^{-5} C/m^2 and 5.7×10^{-5} C/m^2. These values correspond to assuming ε equal to its low (air = 1) and high bounds (polyester = 3.25). They are about two orders of magnitude smaller than the experimental determination of σ_{max}, which is 4.7×10^{-3} C/m^2, obtained by multiplying the fiber coverage in Fig. 2b (1.6×10^{-8} m^3/m^2) times the quotient of the electrospinning current (2.0×10^{-7} A) to the infused polymer volume rate (6.8×10^{-13} m^3/s) for that run. This difference suggests that charge loss is taking place either before the fibers reach the substrate (by ionization or emission of fibrils, so that the fibers hold less charge per unit mass than has been assumed), or, as we believe, after they reach the substrate, either by neutralization by air ions or by conduction along the fibers and substrate threads into the underlying grounded electrode. Charge loss due to electrical breakdown to the grounded electrode (through the voids in the porous substrate) is probably not taking place because the electrical potential across the charged layer $\phi_{max} = \sigma_{max} S/(\varepsilon\varepsilon_o)$ becomes

$$\phi_{max} \approx \frac{V_e R}{L} = 476 \text{ volts} \tag{3}$$

and this voltage is insufficient to trigger air breakdown, since it is much lower than the spark breakdown gap voltage V_{spark} of 1600 V, predicted for $S = 0.24$ mm, for a uniform field between two charged plates in air, using:

$$V_{spark} = aS + b\sqrt{S} \quad (4)$$

where a= 24400 Vcm^{-1} and b = 6530 Vcm$^{-1/2}$ (at 760 Torr, 20 °C, 11 g/m^3 humidity) [30]. Interestingly, these equations imply the existence of a critical substrate thickness $S^*(R)$ at which $V_{spark} = \Phi_{max}$, such that for thinner substrates air breakdown would take place (and fibers would continuously accumulate onto the substrate), whereas for thicker substrates than S^*, σ_{max} would be reached and breakdown would not occur. Note that these concepts may also apply to the situation in which fibers form a mat directly on the grounded electrode.

Other studies in which insulating substrates were coated with electrospun fibers have not reported reduced fiber deposition due to static charging of the substrate. For instance, Kim collected fiber mats on thin PET films (presumably on a grounded electrode) [31]. Mitchell and Sanders [32] formed 0.3 mm thick mats of polyurethane molten micro-fibers over circular insulating substrates (10 and 15 cm diameter Petri dishes) placed at various heights between a grounded plate and the needle separated by 17 cm. Kenawy et al. [33] could "easily" coat a plastic Petri dish and 3-cm polystyrene culture dishes by EVOH fibers, producing a mat "a few fibers thick" in a few minutes. Because these substrates and ours have similar S/R ratios (0.04 for a 10 cm Petri dish, 0.12 for the culture dish, assuming S = 2 mm), equations (1) and (2) would predict similar repulsion fields and saturation surface charge densities as in our study. However, attaining the same surface charge density over the much larger substrates used in these works (relative to our discs) ought to take a much longer time, under similar electrospinning current, and charge loss by conduction is likely to be more effective. On the other hand, Zucchelli et al. [25] have formed >100 μm thick mats of PLLA micro-fibers over steel substrates coated with vitreous enamel (an insulator), and found a correlation between porosity of the fiber mat and the electrical resistance of the enamel substrate.

Finally, we note that on stand-alone insulating substrates (not backed by a grounded electrode), charge saturation and fiber rejection would occur much earlier than when the substrate is placed in front of a grounded electrode. This is because in the absence of image charges, the repulsive field strength E_s caused by accumulated charges on the substrate would be vastly increased, times $\varepsilon R/S$ to about $\sigma/2\varepsilon_o$ (compare to eq. (1)). This observation underscores the usefulness of placing grounded electrodes directly behind dielectric substrates.

3.3. Fiber patterns onto substrates of varying morphology and conductivity

Fig. 2c through h provide examples of non-uniform fiber coverage induced by local variation in surface conductivity and morphology of the substrate, for various substrate materials described in Table 1. Fig. 2c and d correspond to fibers from 18% nylon solution spun for 10 min on discs of F-340 fiberglass mesh, which has very wide openings compared to the P-20 substrate discussed previously. Instead of the random pattern found on P-20 substrates, on F-340 mesh fibers collected in a repeating pattern within each mesh cell. A mass of curled fibers accumulated at the center of each mesh opening, and became surrounded by outer fibers that radiate outward towards the surrounding fiberglass threads. The repetition of the cell pattern is consistent with the idea that the fiber pattern is the result of the effect of the (periodic) electrostatic field on the fiber path during collection. The metal surface exposed through the openings was more attractive to the fibers than the fiberglass threads. This could be due to: (i) repulsion from charge accumulated over the insulating fiberglass threads, and (ii) stronger attraction of the airborne fibers towards induced charge ("image charges") on the grounded metal areas. It is therefore reasonable to infer that local variations in the electric field can influence fiber deposition, and that the field is depressed over the fiberglass regions due to electrostatic charging, and that such charging did not prevent (perhaps even aided) fiber accumulation on the metal surface. Interestingly, the fiber pattern in Fig. 2 c and d is very similar to that reported by Zuchelli et al. [25] for PLLA fibers collecting over dispersed conductive points over insulating substrates (see Fig. 3c in [25]). Both systems show that fibers are preferentially attracted to the conductive regions.

Fig. 2e and f correspond to woven stainless steel mesh substrate S-370, and fibers spun at otherwise the same conditions as for Fig. 2c–d for substrate P-20. In this case, a repeating pattern from cell to cell was again found, but the fibers were now preferentially collected over the wires, which are electrically conductive. Fibers fan out from the mid sections of the mesh wires towards the nearest cross and parallel wires. Since, during spinning, the mesh wires are at the same potential as the underlying grounded cylinder, the conducting wires exert a greater attraction on incoming fibers than the grounded metal areas beneath, since most field lines must end on the raised wire surfaces. As a result, fibers preferentially collect on the wires. This fiber pattern closely resembles that of Morozov and Vsevolodov for electrospun PVP fibers over a floating metal mesh [[24]; fig. 2B], that of Deitzel et al for PEO [[23], fig. 15], and somewhat that of Gibson et al for polyurethane fibers over metal screens [[11]; fig. 6].

Fiber coverage onto larger sheets of nylon mesh also was irregular. Fig. 2g and h show the central region of a 8 cm strip of nylon mesh N-165 coated with fibers. Most fibers are collected along the mesh threads, and a smaller number of fibers lay across the threads over the opening. Interestingly, this pattern somewhat resembles the one found on stainless steel meshes of Fig. 2e and f.

3.4. Ion-assisted fiber collection and fiber thinning

The observations of poor and non-uniform fiber deposition described in Sections 3.1 and 3.3 motivated our development of ion assistance during deposition. During deposition, the substrates were alternatively exposed to charged electrospun fibers and to ions of opposite polarity. Fig. 3a shows the fibers deposited onto a polyester P-20 disc with the assistance of the corona ion source, and at otherwise the same experimental conditions as for Fig. 2a, including deposition time. Compared to Fig. 2a, Fig. 3a shows a dense and uniform coverage. Fig. 3b is a close up of a mat obtained on a P-20 disc under the same conditions as for Fig. 2b except for the use of corona ions in Fig. 3b. Note the much greater concentration of fibers in Fig. 3b relative to Fig. 2b, as well as their random orientations.

To see if this ion-assist method would be effective on substrates having significantly greater openness than the non-woven polyester tested, fiber deposition was attempted on a series of square-woven nylon and polyester meshes which ranged in open area from 33 to 49%, and in thread diameters from 50 to 495 μm, which are described in Table 1. Uniform fiber coverage was consistently obtained on all of these materials. Fig. 3c and d show two examples from these tests: nylon mesh N-165 and polyester mesh P-225. The N-165 substrate has a similar thickness to the P-20 substrate (245 μm), but with 8 ¼ times thicker threads and much wider openings; yet, the fiber collection was equally uniform in both cases. In conclusion, with the assistance of the corona ion source, the fibers showed no sensitivity to the morphology of the underlying substrate, becoming homogeneously distributed over all substrates tested.

To investigate if the electrospun fiber mats lie flat on the substrate, we imaged cross-sections of fiber mats collected over

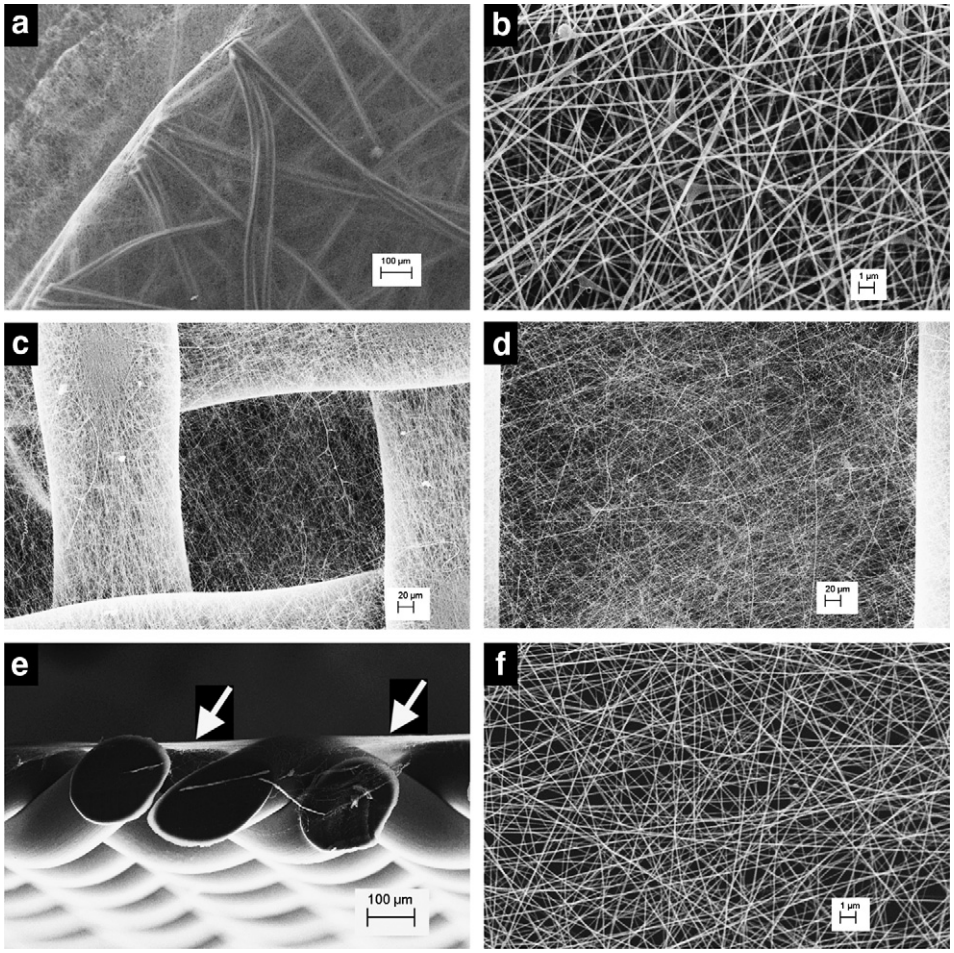

Fig. 3. SEM images of electrospun nylon fibers collected with corona ion assistance onto different substrates: (a) two P-20 discs; (b) six P-20 discs; (c, d) six discs of N-165 mesh; (d) six discs of P-225 mesh; (e) six discs of N-165 mesh (arrows indicate top of fiber mat); (f) N-165, 8-cm wide strip (center of deposition region). Nylon solution concentrations: 19% wt (a), 18% wt (c, d, e), 16% wt (b, f). Collection times: 10 min (*a*, b), 5 min (*c*, d, f), 15 min for (e). $V_e = +7.5$ kV, $V_c = -7.5$ kV for (a) and -5.0 kV for (b–f).

N-165 discs, for which the mesh openings are as wide as the mesh is thick. The sections were cut using a razor blade. The example shown in Fig. 3e in cross section confirms flatness. Note that the cause for the flatness of the fiber mat cannot be stretching of the fibers by the cylinder's rotation, since the fibers arrange themselves in a random pattern instead of in alignment (Fig. 3d).

Similarly to the nylon and polyester substrates, the assistance from corona ions led to uniform fiber coatings over electrically conducting S-370 discs.

Ion assistance on a 8 cm strip of N-165 mesh also resulted in the concentration of fibers in the central region of the substrate where corona ions were aimed (Fig. 3f). Compared to Fig. 2g and h, otherwise taken at the same conditions as Fig. 3f, enhanced fiber deposition is clearly observed in Fig. 3f.

Ion assistance resulted in fibers becoming visibly thinner as the corona voltage V_c was increased (in absolute value). This is illustrated in Fig. 4a and b for corona voltages -2.0 kV and -4.5 kV. Fig. 5 shows that the average fiber diameter data d_F decreased monotonously with the corona voltage $-V_c$, while the standard deviation (SD) of the fiber diameter remained roughly unchanged. A non-increasing SD rules out the scenario in which the fiber diameter decreases by migration of small fibers towards the deposition region, since large increases in SD would accompany the diameter mean reduction. Instead, we believe that the higher corona voltage resulted in more negative corona ions accumulating on the substrate, thus increasing the pull on the airborne positively charged fibers towards the insulating disc and causing them to stretch. From this point of view, the increased numbers of fibers visible in Fig. 4b are expected, both to satisfy mass conservation (because the same mass in thinner fibers requires more fiber length), and because increased fiber mass should collect on the substrate at higher corona voltages. Notice also that the fiber splaying visible in Fig. 4a is consistent with the greater time spent by the airborne fibers in transit between the electrodes.

Fiber thinning has also been reported by Deitzel et al. [34], who confined and accelerated fibers by means of ring electrodes. The thinning was attributed to the greater overall voltage drop when ring electrodes were used (relative to standard spinning), since greater potential drop results in more electrical work on the fibers, resulting in stretching of the fibers. Similarly, in our case, the deposition of negative ions on the substrate causes a lowering of the electrostatic potential on the substrate, thus effectively increasing the electric potential drop experienced by the fibers between the electrospinning needle and the collection surface.

To help further understanding the role played by the corona ions, we examine the process by which steady state is reached. Consider an initial state in which the corona is not on, and the substrate has already become saturated with positive charges (which produce the electric field strength $-E_s$) as explained in Sections 3.1 and 3.2, and does not accept fibers. Let's consider the

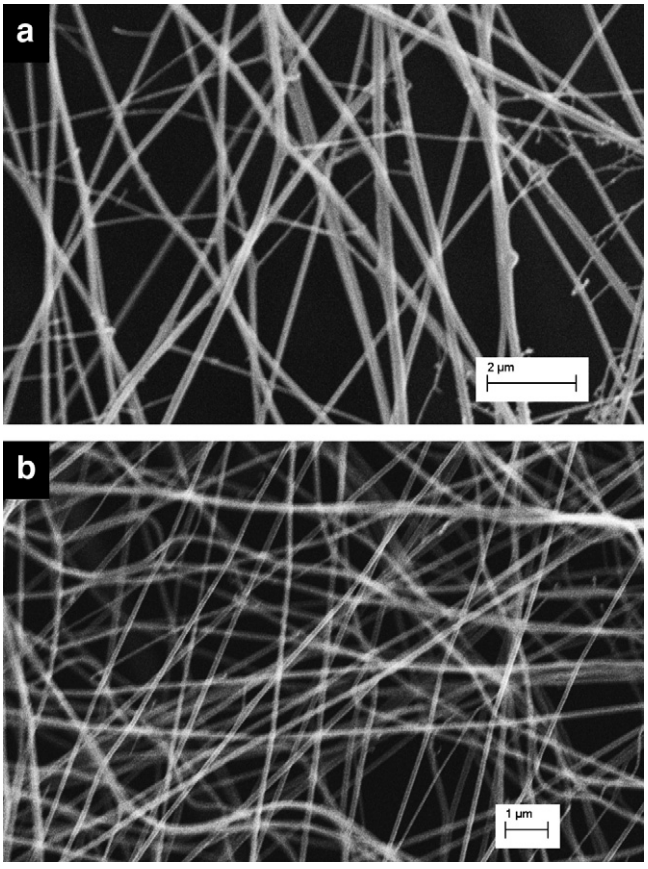

Fig. 4. SEM images of fibers from 16% nylon solution collected on N-165 substrate discs at corona voltages (a) $V_c = -2.0$ kV, (b) $V_c = -4.5$ kV. $V_e = +7.0$ kV, six discs attached to cylinder in each condition, collection time = 5 min, electrospinning current = 202 nA.

changes in substrate net charge after the corona is suddenly turned on. In the first pass of the substrate in front of the corona source, ions will be collected, reducing the substrate's net positive charge. This reduction may or may not be enough to bring the net charge on the substrate to a negative value. Regardless, when the substrate moves back in front of the electrospinning needle, the field component due to the net charge on the substrate E_s will have

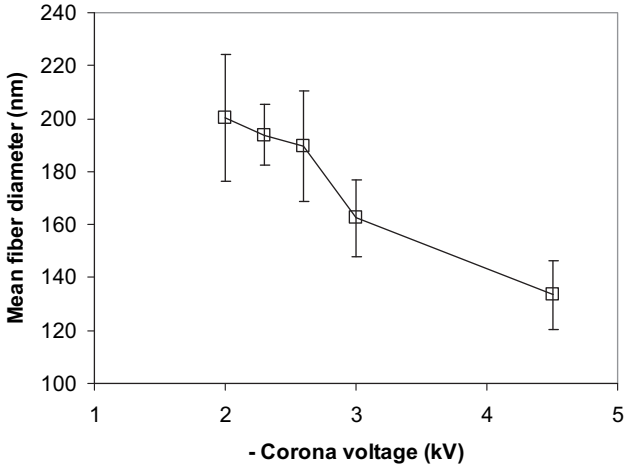

Fig. 5. Dependence of mean fiber diameter on corona needle voltage, for N-165 substrate discs. Other parameters are the same as for Fig. 4. Bars represent ±1 standard deviation. Means are based on 15 measurements on fibers taken randomly from 3 different locations on one disc of a set of six simultaneously coated discs.

weakened relative to its initial, saturation value (eq. (1)). As a result, some fibers will be admitted on the collector at the end of this first rotation of the cylinder. In subsequent cycles, as the substrate becomes less positively charged or even negatively charged, more fibers will collect per cycle. Eventually, the charge level of the substrate will reach a steady state condition at which as much ion charge as fiber charge is collected in each cycle. At this point, the time-average electric potential of the substrate surface passing in front of the electrospinning needle is lower than the initial saturation value (Φ_{max}) before the corona got turned on, thus allowing some fibers to be collected in every cycle, leading to fiber accumulation over time. This picture remains qualitatively the same in the presence of slow leakage from the substrate by conduction to the underlying grounded cylinder.

In conclusion, (i) even a small amount of corona current will lower the net charge on the substrate below its saturation value, thus triggering fiber accumulation; and (ii) as the corona voltage increases, the charge on the substrate becomes less positive, becoming negative at high enough corona voltages. In addition, (iii) the reduced electrostatic potential on the substrate surface results in an increase in the electric field strength, which points towards the substrate. Therefore, the pull on the fibers gets stronger at higher corona voltage values, in qualitative agreement with the monotonous decrease of fiber size with corona voltage shown in Fig. 5.

Eventually, at high enough corona voltages, the negative charge collected on the substrate may be so high as to cause electric breakdown within the substrate (as described in Section 3.2). In fact, we have observed that corona voltages exceeding the reported values sometimes result in damage to the fiber mats, in the form of round dark spots on the fiber mat, which could be due to the onset of electrical discharges.

4. Conclusions

The standard electrospinning of fibers onto substrate surfaces often leads to non-homogeneous coatings. Problematic substrates include types (i) having mixed electrically insulating and conductive regions, and (ii) having uneven morphology, such as grids, meshes, felts, etc, regardless of electrical conductivity. Variations in the electric field above these substrates influence the airborne fibers' paths just before deposition. Two kinds of inhomogeneous fiber coatings were observed: (1) electrostatic repulsion of fibers from small insulating discs (porous polyester and nylon, and solid glass); (2) uneven fiber distributions on insulating and on conducting substrates with a non-flat, porous morphology ('structured materials'), such as felts and meshes. All substrate kinds were mounted over a rotating grounded cylinder.

Electrostatic repulsion happens when the insulating material becomes saturated with charge. The theoretical electric field contribution due to accumulated charge onto an insulating disc was presented, based on the dipolar approximation. The theoretically minimum necessary fiber concentration needed to cause complete fiber rejection was estimated, and this estimate was significantly less than the fibers found to collect on a disc; however, this amount was much less than the fiber accumulation outside the disc. We interpret that the charge needed for repulsion (saturation charge) is nearly met, but not exactly because of charge loss mechanisms, which over time allow the escaping of charge from the collected fibers.

A method was developed to offset electrostatic repulsion effects, as well as the non-uniform patterns that are characteristic of fibers electrospun onto structured materials. The method is based on the rapid, alternating deposition of charged fibers and oppositely charged corona ions, onto the substrates mounted on a rotating

cylinder. With this method, highly homogeneous mats of randomly oriented nanofibers were readily formed on different kinds of substrates tested: insulating non-woven (random) mesh, insulating square-woven mesh, and conducting square-woven mesh. Cross sections of spun-on nylon meshes showed that these fiber mats lie flat on top of meshes, instead of conforming to the underlying substrate topography.

Fiber diameter was found to decrease as corona voltage increased (in absolute value), indicating that the fibers stretch as they are electrostatically pulled towards the substrate. However, it is argued that the substrate may or may not be negatively charged for this effect to happen, that the role of the corona ions is to reduce the charge on the substrate from the saturation level that would be attained without ion collection, and that such charge reduction results in attraction of airborne electrospun fibers towards the substrate region.

Conceivably, the ion assistance approach proposed here could be implemented into other configurations, including scaled-up continuous-production systems [35].

Acknowledgements

Drs. Jordi Grifoll-Taverna (URV), Dmitry Pestov (VCU), Pavel Kiselev (URV), and John B. Fenn (VCU) are gratefully thanked for fruitful discussions on the subject. Financial support from the European Commission for project OPEN ToK (ref. MTKD-CT-2005-030040) is gratefully acknowledged. In addition, JRLl acknowledges financial support from the Spanish Ministry of Science and Innovation (refs. CTQ2008-05758/PPQ and CIT-420000-2008-30) and the Catalonian Government (ref. 2009-SGR-1529).

References

[1] Ahn YC, Park SK, Kim GT, Hwang YJ, Lee CG, Shin HS, et al. Curr Appl Phys 2006;6:1030–5.
[2] Barhate RS, Ramakrishna S. J Membr Sci 2007;296:1–8.
[3] Pham QP, Sharma U, Mikos AG. Tissue Eng 2006;12:1197–211.
[4] Gelain F. Int J Nanomedicine 2008;3(4):415–24.
[5] Scott SA, Bowlin GL. J Mater Chem 2008;18:260–3.
[6] Kenawy E-R, Bowlin GL, Mansfield K, Layman J, Simpson DG, Sanders EH, et al. J Controlled Release 2002;81:57–64.
[7] Kim K, Luu YK, Chang C, Fang D, Hsiao BS, Chu B, et al. J Controlled Release 2004;98:47–56.
[8] Kumbar SG, Nair LS, Bhattacharyya S, Laurencin CT. J Nanosci Nanotech 2006;6:2591–607.
[9] Kessick R, Tepper G. Sensors and Actuators B 2006;117:205–10.
[10] Gibson PW, Schreuder-Gibson HL, Rivin D. AIChE J 1999;45(1):190–5.
[11] Gibson P, Schreuder-Gibson HL. INJ Summer; 2004:34–41.
[12] Wang Z-G, Wan L-S, Liu Z-M, Huang X-J, Xu Z- K. J Mol Catal B Enzymatic 2009;56:189–95.
[13] Bellan LM, Strychalski EA, Craighead HG. J Vac Sci Technol B 2008; 2(5):1728–31.
[14] Burger C, Hsiao BS, Chu B. Ann Rev Mat Res 2006;36:333–68.
[15] Greiner A, Wendorff JH. Angew Chem Int Ed 2007;46:5670–703.
[16] Agarwal S, Wendorff JH, Greiner A. Polymer 2008;49:5603–21.
[17] Thavasi V, Singh G, Ramakrishna S. Energy Environ Sci 2008;1:205–21.
[18] Ma M, Hill RM, Rutledge GC. J Adhes Sci Tech 2008;22:1799–817.
[19] Reneker DH, Yarin AL. Polymer 2008;49:2387–425.
[20] Rutledge GC, Fridrikh SV. Adv Drug Deliv Rev 2007;59:1384–91.
[21] Shin YM, Hohman MM, Brenner MP, Rutledge GC. Appl Phys Lett 2001; 78(8):1149–51.
[22] Deitzel JM, Beck Tan NC, Kleinmeyer JD, Rehrmann J, Tevault D, Reneker D, et al. Army Research Laboratory 1999. Report ARL-TR-1989.
[23] Deitzel JM, Kleinmeyer J, Harris D, Beck Tan NC. Polymer 2001;42:261–72.
[24] Morozov VN, Vsevolodov NN. Adv Mater 2007;19:4381–6.
[25] Zucchelli A, Fabiani D, Gualandi C, Focarete ML. J Mater Sci 2009;44:4969–75.
[26] Morozov VN, Morozova TY, Kallenbach NR. Int J Mass Spectrom 1998;178: 143–59.
[27] Bender F, Wächter L, Voigt A, Rapp M. Proceedings of IEEE Sensors; 2003:115–9. ISBN 0-7803-8133-5.
[28] Bergshoef MM, Vancso GJ. Adv Mater 1999;11(16):1362–5.
[29] Huang C, Chen S, Lai C, Reneker DH, Qiu H, Ye Y, et al. Nanotechnology 2006;17:1558–63.
[30] Blair DTA. In: Meek JM, Craggs JD, editors. Electrical breakdown of gases. Chichester: John Wiley & Sons; 1978. Chap. 6.
[31] Kim GH. J Polym Science Part B Polym Phys 2006;44(10):1426–33.
[32] Mitchell SB, Sanders JE. J Biomed Mater Res Part A 2006;78A(1):110–20.
[33] Kenawy E-R, Layman JM, Watkins JR, Bowlin GL, Matthews JA, Simpson DG, et al. Biomaterials 2003;24:907–13.
[34] Deitzel JM, Kleinmeyer JD, Hirvonen JK, Beck Tan NC. Polymer 2001;42: 8163–70.
[35] Zhou F-L, Gong R-H, Porat I. Polym Int 2009;58:331–42.